INVESTIGACIÓN REVISTA MEXICANA DE FÍSICA **56** (4) 297–301 AGOSTO 2010

Formation and characterization of ion beam assisted nanosystems in silicon

P.R. Poudel[a], B. Rout[a], K.M. Hossain[a], M.S. Dhoubhadel[a], V.C. Kummari[a], A. Neogi[b], and F.D. McDaniel[a,*]
[a] *Ion Beam Modification and Analysis Laboratory, Department of Physics, University of North Texas, 1155 Union Circle#311427, Denton, Texas 76203, USA.*
[b] *Ultrafast Spectroscopy and Nanophotonics Laboratory, Department of Physics, University of North Texas, 1155 Union Circle#311427, Denton, Texas 76203, USA.*

Recibido el 28 de enero de 2010; aceptado el 21 de mayo de 2010

Even though silicon is optically inactive, the nanoscale particle structures (*e.g.* SiC) in Si or silica matrices are potential candidates for light emitting solid state device applications with higher operation temperatures. The synthesis of these nanostructures involves ion implantation and subsequent thermal annealing. The film thicknesses and sizes of the nanostructures can be controlled by ion energy, fluence, and annealing conditions. Particle accelerator based characterization was used at different stages of formation and analysis of these nanosystems in Si. Results will be presented using infrared spectroscopy (IR), X-ray diffraction spectroscopy (XRD), and photoluminescence (PL) spectroscopy.

Keywords: SiC; nanosystems; ion implantation; photoluminescence.

Aunque el silicio es ópticamente inactivo, las estructuras de las partículas a nanoescala (por ejemplo, carburo de silicio) en Si o en la matriz de sílice son candidatos potenciales para aplicaciones de dispositivos emisores de luz de estado sólido con temperaturas de operación mayores. La síntesis de estas nanoestructuras implica la implantación de iones y de recocido térmico posterior. Los espesores de película y tamaños de las nanoestructuras pueden ser controladas por la energía de iones, flujo de energía y las condiciones de recocido. Una caracterización basada en un acelerador de partículas se utilizó en las diferentes etapas de la formación y el análisis de estos nanosistemas en Si. Los resultados se presentarán mediante espectroscopía de infrarrojos (IR), X-espectroscopía de difracción de rayos X (DRX), y espectroscopía de fotoluminiscencia (PL).

Descriptores: SiC; nanosistemas; la implantación de iones; fotoluminiscencia.

PACS: 85.60.-q; 85.30.-z; 68.55.Ln

1. Introduction

Silicon is highly successful as an electronic material, however the indirect band gap makes it, a poor material for optoelectronic applications [1]. With the reporting of visible light emission from porous silicon in 1990 [2-3], additional research has been carried out to explore the possibility of light emission from nanoscale structures based on Si technology-compatible media, such as silicon dioxide (SiO_2) [4-5]. Since then, photoluminescence (PL) has been observed from various Si based nanomaterials such as Si-, Ge-, C-, and SiC-nanocrystals embedded in SiO_2 [6-7]. Such investigations of silicon based nanosystems pave the way to propose silicon-based materials for photonic applications. The SiC nanocrystal structures [8] are very promising materials for the substitution of silicon in the electronic industry due to its wide band gap, high breakdown electric field, high thermal conductivity, and thermal stability [9]. These remarkable features of SiC nanocrystals make them useful for high temperature, high power, and high frequency electronics [10]. These materials have been studied extensively over the past decade as a potential candidate for nanoscale light emitters for the blue and ultraviolet spectral ranges [11-13]. The SiC nanostructures have also been found as negative index metamaterials, that can be applied for the enhancement of the resolution of near-field imaging via the superlensing effect [14].

There has been considerable progress made in the studies that involve the synthesis and characterization of nanometer sized structures in Si and the silica (SiO_2) matrix. The studies on the optical properties of such nanostructures have been motivated by the observed variation in the band gap with the size of the nanostructure [15-16], which allows the tuning of luminescence wavelengths for the desired applications.

Silicon carbide, which is a material of interest, is a wide, optically indirect, band gap semiconductor exhibiting a weak PL signal. The SiC-based LED intensity is low with a very low quantum efficiency of approximately 10^{-4} [7]. Therefore, the enhancement of luminescence in these compound semiconductor materials is strongly desired. One technique to enhance the luminescence and increase the quantum efficiency of the LED is through the fabrication of material on the nanometer scale.

Many techniques such as molecular beam epitaxy (MBE) [17], sputtering, and plasma enhanced chemical vapor deposition (CVD), colloidal suspensions [18], and ion implantation [19], to name a few, have been employed in the formation of nanoclusters. Among these techniques, the advantages of precise and predictable control of the quantity and distribution of doping impurities and the complete compatibility with silicon-based technology indicate that ion implantation is a quite suitable way to fabricate silicon-based light emitting materials [20-21]. In this paper, the steps involved in the formation of SiC nanocrystals through low-energy carbon ion implantation into silicon are discussed. The possible light emissions from carbon implanted into thermally grown silicon dioxide are also discussed.

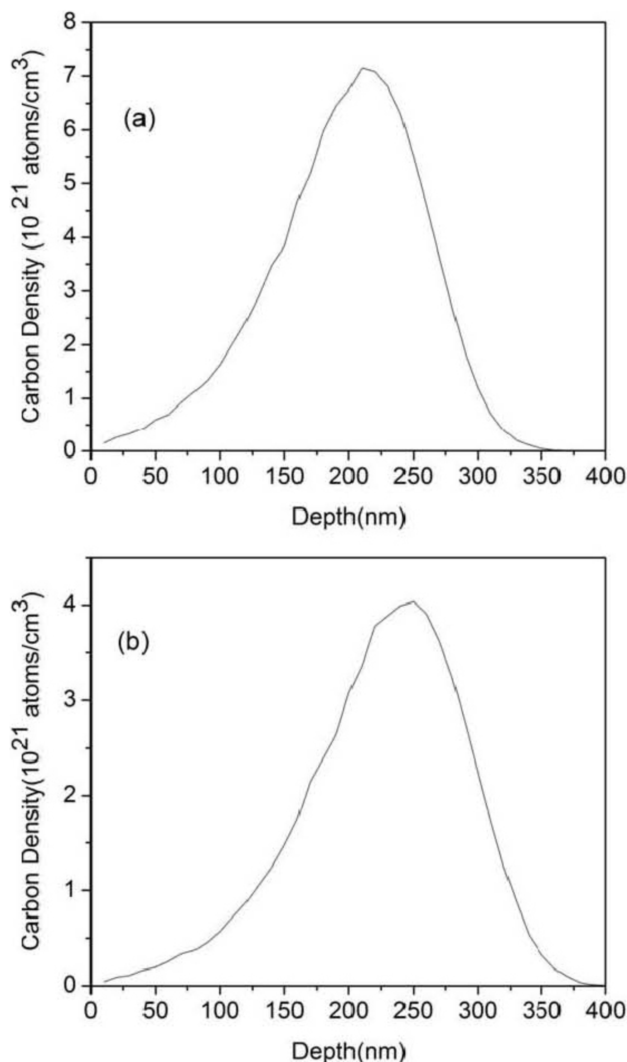

FIGURE 1. SRIM simulation of the implantation profile of (a) 1×10^{17}atoms/cm^2 fluence of 65 keV carbon ion beam into Si and (b) 6×10^{16} atoms/cm^2 fluence of 70 keV carbon ion beam into SiO_2.

2. Experimental

P-type Si (100) substrates were used as the starting materials. Before ion implantation, the silicon substrates were cleaned with acetone in order to remove the surface contaminants on the sample. The substrates were etched in a dilute HF solution in order to remove the native oxide layer on the silicon surface. Some of the silicon wafers were oxidized in a conventional furnace by a wet oxidation method in order to grow the silicon dioxide layer of around 400 nm thickness. The thermally grown silicon dioxide samples were implanted with a 70 keV negatively-charged carbon beam (C^-) to a fluence of 6×10^{16} atoms/cm^2 and the virgin silicon samples were implanted with 65 keV C^- ions to a fluence of 1×10^{17} atoms/cm^2 by using the low energy ion implantation facility at the Ion Beam Modification and Analysis Laboratory (IBMAL) at the University of North Texas. Low current densities were maintained in order to avoid the sample heating during the ion implantation. A National Electrostatics Corporation (NEC) cesium negative ion sputter source (SNICS-II) associated with a 3 MV Tandem Pelletron Accelerator system (9SDH-2) was used for the ion implantation [22]. The typical beam current was $\sim$1 μA (beam flux $\sim 2\times10^{12}$ atoms/s cm^2) during the ion implantation. During the ion implantation, the residual gas pressure in the experimental chamber was maintained at $\sim1\times10^{-7}$ torr. The implantation profile of the carbon ions were simulated using a Monte Carlo method based simulation code (The Stopping and Range of Ions in Matter, SRIM-2008) [23]. For the 65 keV C^- ion implantation into Si, the projected range (Rp) and straggling of the ions was simulated to be 190 nm and 60 nm, respectively, where as the projected range and straggling of 70 keV carbon ions into silicon dioxide was simulated to be 220 nm and 62 nm, respectively. The simulated implantation profile of C^- ions in Si and silicon dioxide substrates by using the SRIM code are shown in Fig. 1a and 1b, respectively.

The conventional furnace annealing was performed at 1100 °C for 1 hr in a gas mixture (4% H_2 + 96% Ar) for carbon implanted into silicon samples, whereas, the samples with carbon implanted into silica were annealed at 800 °C for 25 min. The phase formation of SiC in the silicon substrate was characterized by using a Rigaku X-ray diffractometer. The sample was further characterized by Fourier Transformed Infrared Spectroscopy (FTIR). The carbon implanted silica samples were characterized by FTIR, Raman spectroscopy and photoluminescence (PL) spectroscopy. The infrared absorption spectra were recorded using a 750 Nicolet FTIR with 4 cm^{-1} resolution. Raman measurements were performed by using A Thermo-Electron Almega XR with a 532 nm (green) laser. The high sensitivity, TE-cooled silicon CCD array detector was used to detect the Raman signal. Room temperature PL measurements were carried out by using 325 nm He-Cd laser as a source of excitation. The PL spectra were recorded with a CCD detector.

3. Results and discussion

3.1. Carbon implanted into silicon

The X-ray diffraction pattern of the silicon sample implanted with 65 keV C^- to a fluence of 1×10^{17} atoms/cm^2 and the sample annealed at 1100 °C for 1 hr are shown in the Fig. 2. The XRD pattern of the as-implanted and annealed samples are labeled as (a) and (b) respectively. The appearance of the broad peaks in the 25-35° and 45-60° range indicates the ion beam induced amorphization in the implanted Si matrix. However, the diffraction from (111), (220) and (311) planes of Si along with the diffraction peak (centered at 35.5°) from (111) plane of β-SiC (Cubic SiC with Zincblend lattice structure) are clearly seen in the diffraction pattern (b) of Fig. 2. This indicates the re-crystallization of the ion beam damaged Si layer during high temperature annealing. The average size

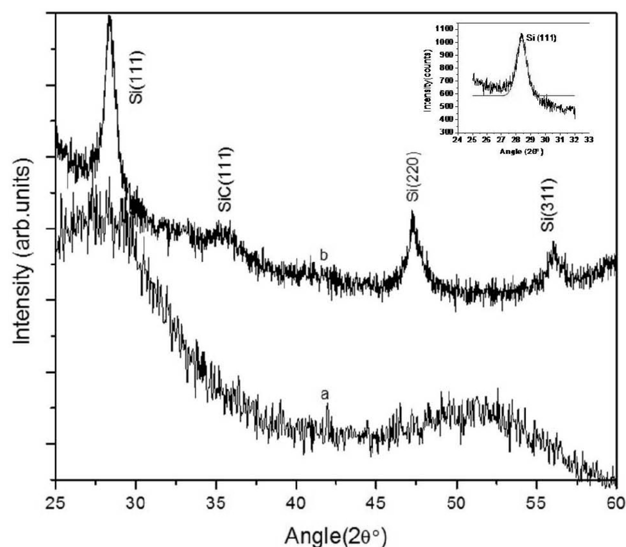

FIGURE 2. X-ray diffraction pattern of (a) the as implanted sample and (b) the sample annealed at 1100 °C for 1 hour. The 1×10^{17} atoms/cm^2 fluence of carbon was implanted into silicon.

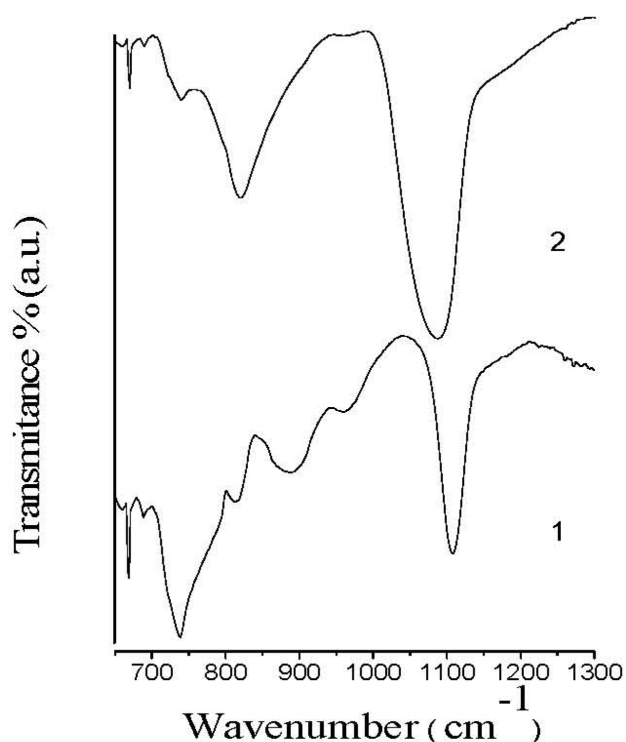

FIGURE 3. FTIR Transmittance spectra of the silicon (1) as-implanted sample and (2) the sample annealed at 1100 °C for 1 hour. The 1×10^{17} atoms/cm^2 fluence of carbon was implanted into silicon.

of nanocrystalline Si formed after annealing is found to be $\sim$ 11 nm. To determine the average crystalline size, the Si (111) peak centered at 28.35° was fit with a Gaussian peak as shown in the Fig. 2 inset. The FWHM of the peak was then inserted into Scherrer's formula, $P = (0.9\lambda)/(B\cos\theta)$, to calculate the average particle size of the Si crystallites. In Scherrer's formula P(Å) is the size of the crystallites, λ(1.54Å) is the wavelength of Cu K_α radiation, B (radians) is the full width half maximum (FWHM) of the diffraction peak, and θ is the Bragg angle. As inferred from the diffraction spectra, the β-SiC peak centered at 35.5° has very low intensity and a Gaussian fit to determine the average crystalline size is difficult.

The FTIR spectra of the as-implanted sample (1) and the sample annealed at 1100 °C for 1 hr (2) are shown in Fig. 3. As seen in the transmittance spectra, the band centered at around 736 cm^{-1} is observed for the as-implanted sample. This is the characteristic absorption band for amorphous SiC [24]. The band shifts to higher wave number and

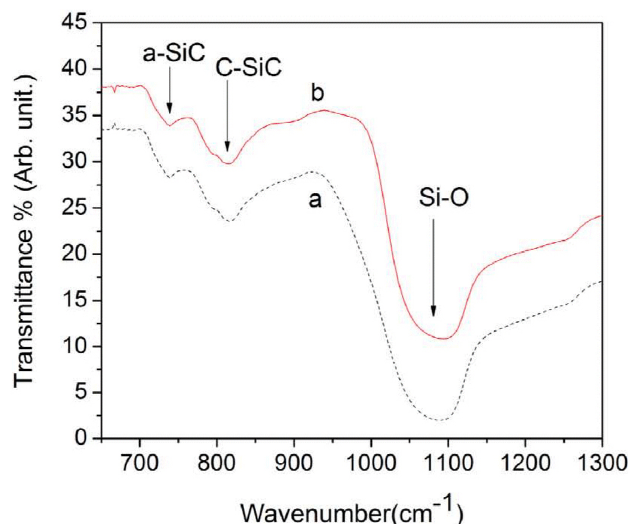

FIGURE 4. FTIR Transmittance spectra of the silica (a) as-implanted sample and (b) the sample annealed at 800 °C for 25 min. The 6×10^{16} atoms/cm^2 fluence of carbon was implanted into silicon dioxide.

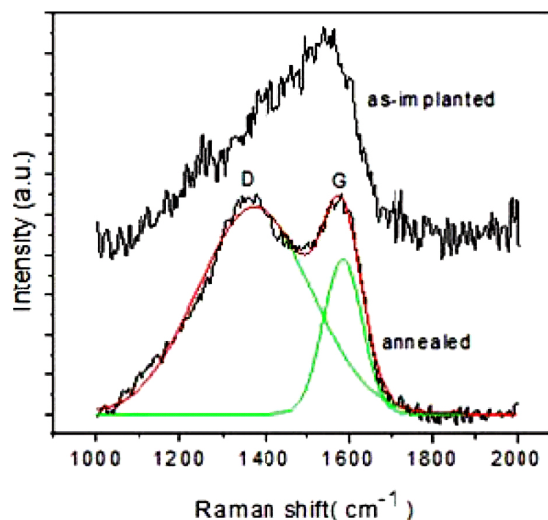

FIGURE 5. Raman spectra of the as-implanted sample and the sample annealed at 800 °C for 25 min. The 6×10^{16} atoms/cm^2 fluence of carbon was implanted into silicon dioxide.

is centered at around 800 cm^{-1} after the sample was annealed at 1100 °C for 1 hour. The band centered at 800 cm^{-1} is a typical band seen for the crystalline β-SiC phase [24]. In addition, there is another absorption dip around 1108 cm^{-1} due to the presence of Si-O bonds in the samples. The absorption dip at around 1108 cm^{-1} in the as-implanted sample is due to the native oxide in the sample. The intensity of this absorption dip increases and shifts to a lower wavenumber after annealing. The increase in intensity is due to the formation of a small amount of oxide during furnace annealing, and the shifting of the absorption dip to lower wavenumber is due to the formation of silicon sub oxide (SiO_x, $0<x<2$) [25]. These bands can be removed by etching the surface oxide layer in buffered HF acid. Removal of the oxide layer doesn't affect the SiC absorption band.

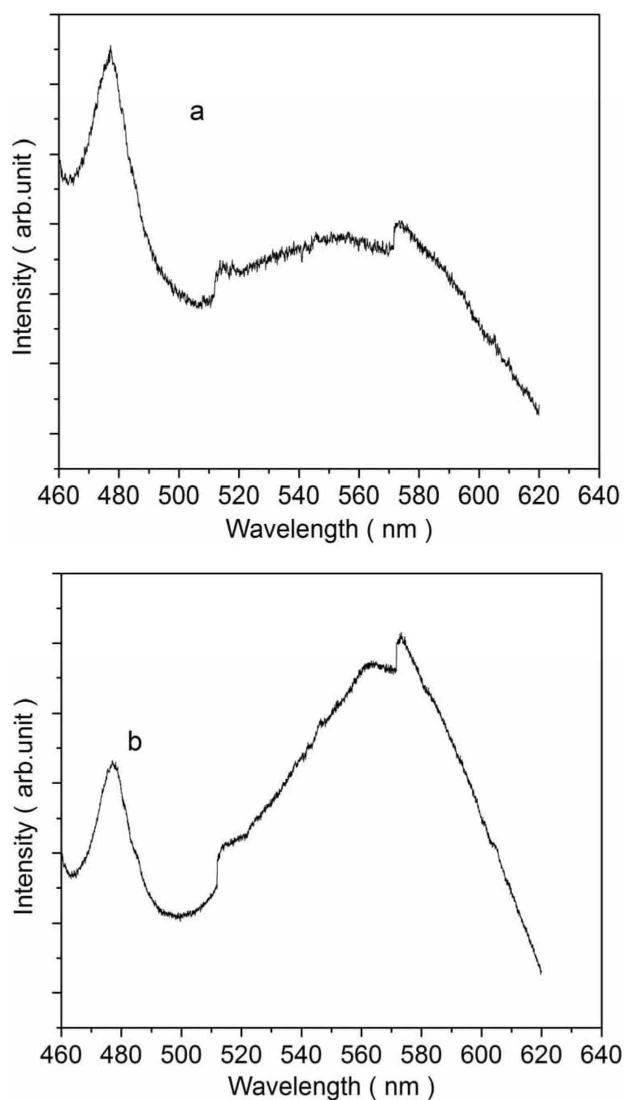

FIGURE 6. Room temperature photoluminescence from the sample (a) the as-implanted sample and (b) the sample annealed at 800 °C for 25 minutes. The sample was silica implanted with 70 keV carbon at a fluence of 6×10^{16} atoms/cm^2.

3.2. Carbon implanted into silica

The FTIR spectra of both the as-implanted (a) and annealed samples (b) of 70 keV C^- at a fluence of 6×10^{16} atoms/cm^2 in silica annealed at 800 °C for 25 min. are shown in Fig. 4, respectively. There is no considerable shift in the absorption dip between the as-implanted and the annealed samples. In both samples, the absorption bands for both the amorphous Si-C bond ($\sim$ 736 cm^{-1} wave number) and the crystalline Si-C bond ($\sim$800 cm^{-1}) were observed. The crystalline Si-C bond in the as-implanted sample might be due to the ion irradiation induced re-crystallization. The existence of the amorphous SiC phase in the annealed sample could be due to the insufficient annealing temperature or insufficient time to form the complete crystalline SiC phase in the sample.

Further structural analysis was performed on the carbon implanted silica sample through the Raman spectroscopy technique and is shown in Fig. 5. In the as-implanted sample, carbon exists mainly in an amorphous form as seen from a single broad band in the range of 1300-1700 cm^{-1} [26]. After annealing the sample, two clearly distinguishable peaks called the D peak with a lower value of raman shift and the G peak with a higher value of raman shift appear. The appearance of these two peaks indicate the presence of sp^2 bonded carbon nanoclusters (graphite like clusters) in the sample [26]. To determine the average cluster size in the annealed sample, the intensities of the D and G peaks were determined by Gaussian curve fitting as shown in Fig. 5. The calculated intensities were applied to the equation L_a=44(I(G)/I(D)) [27], where L_a is the cluster size in angstroms (Å). The average size of the carbon cluster was found to be 32 Å.

No PL is observed from SiC for C implanted into Si, which is formed at a depth of 190-200 nm from the surface in bulk Si. At 300 K, the bandgap in bulk silicon is 1.1 eV, which is significantly lower than the expected PL energy of any SiC nanoparticles emitting in the visible or near-IR wavelength regime (400-1000 nm). This results in the absorption of light emission from the SiC nanoparticles formed within the Si matrix. This narrow bandgap of silicon also results in an absorption of the incident pump laser and reduces the excitation density. However, as silica has a wider bandgap, the pump laser and the PL are not absorbed by the surrounding medium and results in strong light output as discussed below.

The room temperature PL measurements for silica are shown for the as-implanted sample (Fig. 6a) and for the sample annealed at 800 °C for 25 min. (Fig. 6b). The two luminescence bands were observed on both the as-implanted and the annealed samples. There is no considerable change in the intensity of the luminescence band peaked at around 480 nm (blue-green) between the as-implanted and the annealed samples. The broad band in the region of 520-620 nm (covering the upper green to orange light emission) appears more intense after annealing. The increase in the crystalline quantity by the clustering of implanted carbon ions after an-

nealing might be one of the reasons of increased intensity in the broad band emission.

Previous reports [7,19] suggest crystalline SiC as the possible origin of the blue-green band ($\sim$480 nm). Yu *et al*., [28] attributes the 480 nm band to the defect states in silicon dioxide. Previous research works [7,28,29] on carbon implanted into silica also observed the broad photoluminescence band, similar to the 520-620 nm band in the present study, and attributed carbon nanoclusters as the possible origin of emission. Therefore, the complete nature of the origin of those bands in our samples is yet to be determined. However, from the results obtained from FTIR and Raman spectroscopy on carbon implanted silica, we roughly assign the 480 nm band to SiC and broad band (520-620 nm) to carbon nanoclusters.

4. Conclusion

The synthesis of silicon carbide was carried out in p-type Si (100) by using 65 keV carbon ion (C^-) implantation at room temperature. The post implantation annealing was carried out in order to anneal out implantation induced defects and to produce silicon carbide precipitates embedded in the silicon matrix. The Fourier transform infrared spectroscopy analysis and X-ray diffraction studies confirm the formation of the cubic phase (β-SiC). The visible photoluminescence at room temperature in carbon implanted thermally grown silica was observed. The structural characterizations on the carbon implanted silica sample through FTIR and Raman spectroscopy indicate the possible presence of SiC and carbon nanoclusters in the sample. The SiC and the carbon clusters are suggested as the origins of the photoluminescence band centered at 480 nm, and the broad band (520-620 nm) covering the upper green to orange, respectively. The future work involves the light emission measurements on carbon implanted into silicon samples and the detailed structural properties through transmission electron microscopy on carbon implanted silica samples to further distinguish the origins of emissions from the samples.

Acknowledgements

The Work at UNT is supported in part by the National Science Foundation and the Robert A. Welch Foundation.

∗. Phone: 940-565-3251; fax: 940-565-2227; e-mail: mcdaniel@unt.edu

1. S.Godefroo *et al.*, *Nature Nanotechnology* **3** (2008) 174.
2. L.T. Canham, *Appl. Phys. Lett.* **57** (1990) 1046.
3. V. Lehmannand and U. Gosele, *Appl. Phys. Lett.* **58** (1991) 856.
4. L. Brus, *J. Phys. Chem.* **98** (1994) 3575.
5. A.G. Cullis, L.T. Canham, and P.D.J. Calott, *J. Appl. Phys.* **82** (1997) 909.
6. M. Righini, A. Gnoli, L. Razzari, Ugur Serincan, and Rasit Turan, *J. of Nonoscience and Nanotechnology* **8** (2008) 823.
7. Dihu Chen *et al.*, *Optical Materials* **23** (2003) 65.
8. Y.S. Katharria, F. Singh, P. Kumar, and D. Kanjilal, *Nucl. Instrum. Methods B* **254** (2007) 78.
9. J.C. Zolper and M. Skowronski, *MRS Bull* **30** (2005) 273.
10. M.M. Rodriguez *et al.*, *J.Mater Sci: Mater. Electron* **19** (2008) 682.
11. T.V. Torchynska *et al.*, *Microelectronics* **36** (2005) 536.
12. L.S. Liao, X.M. Bao, Z.F. Yang, and N.B. Min, *Appl. Phys. Lett.* **66** (1995) 2382.
13. Z.G. Wang *et al.*, *Nucl. Instrum. Methods B* **191** (2002) 396.
14. D. Korobkin, Y. Urzhumov, and G. Shvets, *J. Opt. Soc. Am. B* **23** (2006) 468.
15. A.P. Alivisatos, *MRS Bulletin* **20** (1995) 23.
16. J.O. Orwa, J.C. McCallum, S. Prawer, K.W. Nugent, and D.N. Jamieson, *Diamond and Related Materials* **8** (1999) 1642.
17. N.N. Ledentsov *et al.*, *Solid-State Electronics* **40** (1996) 785.
18. O.I. Micic *et al.*, *J. Phys. Chem. B* **101** (1997) 4904.
19. L.J. Mitchell, F. Naab, O.W. Holland, J.L. Duggan, and F.D. McDaniel, *J. of Non-Crystalline Solids* **352** (2006) 2562.
20. E. Rimini, *Ion Implantation: Basic to Device Fabrication* (Kluwer Academic, Dordrecht, 1995) p. 19.
21. Y. Maeda, K. Umezawa, Y. Hayashi, K. Miyake, and K. Ohashi, *Thin Solid Films* **381** (2001) 256.
22. R. Middleton, *A Negative Ion Cookbook*, HTML Version: M. Wiplich (October 1989) http://tvdg10.phy.bnl.gov/COOKBook
23. J.P. Biersack and L.G. Haggmark, *Nucl. Inst. and Meth.* **174** (1980) 257, recently updated, the package and its documentation are available at http://www.srim.org.
24. J.A. Borders, S.T. Picraux, and W. Beezhold, *Appl. Phys. Lett.* **18** (1971) 509.
25. Z. An *et al.*, *J. Vac. Sci. Technol. B* **21** (2003) 1375.
26. R. Walker, S. Prawer, D.N. Jamieson, and K.W. Nugent, *Diamond and Related Materials* **8** (1999) 2159.
27. D.S. Knight and W.B. White, *J. Mater. Res.* **4** (1989) 385.
28. Y.H. Yu, S.P. Wong, and I.H. Wilson, *Physica Status Solidi (a)* **168** (1998) 531.
29. S. Hayashi, M. Kataoka, and K. Yamamoto, *Jpn. J. appl. Phys.* **32** (1993) 274.